Case Studies in Thermal Engineering 49 (2023) 103174

Contents lists available at ScienceDirect

Case Studies in Thermal Engineering

journal homepage: www.elsevier.com/locate/csite

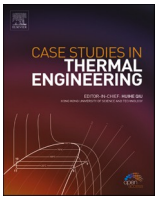

Thermal case classification of solar-powered cars for binary tetra hybridity nanofluid using Cash and Carp method with Hamilton-Crosser model

Tanveer Sajid [a], Wasim Jamshed [a,*], Nek Muhammad Katbar [b,c], Mohamed R. Eid [d,e], Assmaa Abd-Elmonem [f], Nesreen Sirelkhtam Elmki Abdalla [f], Sayed M. El Din [g], Gilder Cieza Altamirano [h,i]

[a] Department of Mathematics, Capital University of Science and Technology (CUST), Islamabad, 44000, Pakistan
[b] Mehran UET Shaheed Zulfiqar Ali Bhutto Campus Khairpur, Pakistan
[c] School of Mathematics and Statistics, Central South University, Changsha, 410083, China
[d] Department of Mathematics, Faculty of Science, New Valley University, Al-Kharga, Al-Wadi Al-Gadid, 72511, Egypt
[e] Department of Mathematics, Faculty of Science, Northern Border University, Arar, 1321, Saudi Arabia
[f] Department of Mathematics, College of Science, King Khalid University, Abha, Saudi Arabia
[g] Center of Research, Faculty of Engineering, Future University in Egypt New Cairo, 11835, Egypt
[h] Universidad Nacional Autónoma de Chota, Cajamarca, Peru
[i] Fizmako Research Group, Bogotá, Colombia

ARTICLE INFO

Handling Editor: Huihe Qiu

Keywords:
Solar sports car
Solar sheet
Reiner-Philippoff tetrhybrid nanofluid
Thermal radiation
Heat generation

ABSTRACT

Solar energy is the most important source of thermal energy that comes from the sun. This kind of energy has enormous potential applications in fields of technology such as photovoltaic panels, renewable power, solar light poles, and solar pumps used for water extraction. The era in which we are living is all about the applications of solar energy in industrial sectors most importantly in solar sports car manufacturing. This article presents a new way of thinking about the heat transport analyses of photovoltaic hybrid vehicles, by factoring Casson-Sutterby liquid with the inclusion of various effects like variable thermal conduction, thermal radiation, heat generation, and tetrahybrid nanoparticles. To solve the modelled equations in regards to both momentum and energy, another well-computational approach known as the Cash and Carp method was used. The effects of a wide variety of factors on temperature, shear stress, and velocity fields, as well as the surface drag coefficient and Nusselt number, are briefly described and illustrated in the form of tables and figures. It then found that the thermal radiation, heat production, and thermal conductivity parameters and insertion of agglomerative tetrhybrid nanoparticles in the base fluid amplify heat transfer rate, it has been shown that the performance of the solar car increases in terms of heat transition. In comparison to standard nanofluid, tetrahybrid nanofluid is the most effective medium for the transmission of heat. From the regression analysis, it is observed that the error in terms of Nusselt number is smaller 0.0151 for the case $\varepsilon = 1.5$, and increases to 0.0151 in the case of $\varepsilon = 2.5$. Relative percentage error is smaller 4.62% in the case of heat generation $Q = 0.7$ but a maximum of 15.8% in the case of thermal radiation $Rd = 2$.

* Corresponding author.
E-mail address: wasiktk@hotmail.com (W. Jamshed).

https://doi.org/10.1016/j.csite.2023.103174
Received 23 February 2023; Received in revised form 1 June 2023; Accepted 7 June 2023
Available online 7 June 2023

1. Introduction

According to all scenarios of efficiency increases of solar power in formerly agricultural regions, ground renewable power advancements are increasing in modern agriculture. A sun will constantly split water, let it dissipate in its heat, let it cool completely, and afterward gather the liquid that has been left behind. These are employed in places that lack access to potable water. The next step is to expose the dirty water or plant material to sunshine, which results in the production of clean water. Many solar creatures also create sunscreens. Water that has not been purified still seems to be available in something like a solar system other than the collectors, and this water is evaporated either by sunlight that is clear or by transparent plastic. Solar power is boosted by the most cutting-edge and environmentally friendly technology. These methods, on the other hand, are highly reliant on the weather, which results in temporal lags here between the supply of sources and their utilization. Renewable heat may be converted into steam for use in a variety of processes, including the desalination of salt water, the sterilization of waste, and the creation of power [1,2]. Nanotechnology has been instrumental in achieving significant improvements in the effectiveness of these systems [3]. The incorporation of suitable nanofluids might bring helpful advances which might contribute towards the equipment's capacity for accurate functioning. The accuracy of the systems may be improved by a factor of approximately 300 if nanocrystals are included in plasmatic nanoliquids. Nanofluids containing carbon nanotubes are the optimal selection for use in solar steam generating systems. Wang et al. [4] deployed nanoliquid in a solar immediate vapor atmosphere that examined the effects of renewable power density and nanoliquid levels on the system. They were also successful in accelerating the pace of condensation, which they did by maximizing the quantity of nanofluid and even the energy provided by the sun.

Solar cars provide a number of advantages over conventional automobiles. It helps reduce the cost of fuel. Solar energy is affordable and abundant. The only extra cost is the expense of a new battery. Solar cars contribute to a better society by totally eliminating the risk of carbon release due to their sustainability and environmental compatibility. It promotes a pollution-free environment by wholly eliminating both air pollution and noise pollution. The major criteria that influence a purchaser's decision to purchase a hybrid vehicle are an advancement within the vehicle's airflow features and then a suitable decrease in ultimate load. The energy coming from the sun is gaining popularity as a viable option since it is advantageous to the atmosphere, it is inexpensive, and it will never run out. Nevertheless, the price tag is only one of the primary barriers that prevent further development of something like solar array plates. Strengthening the thermodynamic functioning of solar array plates can help reduce a few difficulties associated with just this issue. This has been established that nanocomposites do have a fair ability to increase the efficiency of solar panels. Researchers across the world are working on nanofluid flow inside the PV cells of solar panels with the utilization of different kinds of nanoparticles in order the enhance the thermal efficiency of the solar panel to store thermal radiations coming from the sun effectively [5,6].

Because of the outstanding thermal and movement characteristics of nanofluid, it has been projected that this particular liquid would be the subject of extensive study all over the world. Conventional thermal conveyance mediums do not possess these capabilities. Such potent nanofluids function effectively with enhanced thermal conductivity at lower agglomeration of nanoparticles, which are present throughout the liquid. Additionally, it is used in the handling of clinical waste, welding, greasing, power electronics, spacecraft, aviation equipment, and indeed the thermo synchronization of automobiles. The use of nanotechnology to improve heat transmission is currently being researched and developed by a large number of investigators. Considering enhanced heat flow circumstances, existing temperature deliverance mechanisms are incapable of being reached owing to the intrinsically low thermal conductivity. For the preceding ten years, a significant amount of research conducted on a novel method for enhancing thermal performance in liquids by using microparticles. Additionally, Choi [7] coined the term "nanofluid" in order to examine the thermal sedimentation in the working fluids with something like a greater degree of accuracy via the dispersion of these kinds of nanometric solid particles. Initial investigations of nanofluids using a variety of base liquids glycol, water, and waxes estimated viscidity and heating permeability and found that all these nanofluids characteristics were enhanced in comparison to the premised liquids [8–12]. The electric transmittance of dendrimer particles (Cu, Ag, Al_2O_3, TiO_2, CNT, etc.) and propagation through several based liquids (water, PG, grease, oil of palm plant, Oil from coconut plant, etc.) has indeed been evaluated for various temperatures typically range at fractional size and shape of such atoms [13–15]. This is in addition to the heat transfer performance and viscidity of such molecules. For readers' interest similar research on nanofluids was reported by researchers mentioned in Refs. [16–26].

There seems to be a great deal of investigation further into the manufacture of contemporary nanofluids; these kinds of fluids are thought to those as ternary nanofluids (THNF). THNFs have enhanced heat transfer characteristics as a consequence of the associations of several constituents, which has a cumulative effect on the system as a whole. Researchers all over the world investigated ternary hybrid nanofluid due to its better heat transfer rate in comparison to ordinary hybrid nanofluid. Adun et al. [27] investigated various aspects of ternary hybrid nanofluid and their effect on fluid. The effect of ternary hybrid nanoparticles on radiative couple stress fluid moving subjected to a porous medium along with convective boundary conditions was investigated in detail by Sneha et [28]. Goud et al. [29] investigated variable thermal conductivity impact on THNF moving inside the dovetail fin. Nasir et al. [30] investigated THNF impact on magnetized couple stress liquid. Cao et al. [31] scrutinize mixed convective THNF embedded with radiate heat flux and surface slip phenomenon. The effect of stagnation point on magnetized ternary hybrid nanofluid past a cylinder having a convectively heated surface embedded with a heat source as well as the suction effect was investigated in detail by Mahmood et al. [32].

The adoption of renewable sources of power is a strategy for addressing the present worldwide environmental disaster and is an essential component in the process of shielding the environment from dangerous pollutant materials and the discharge of various types of gases. Because the topic is addressed in a broad sense to raise the precision of industrial automation in improving operational and ecological resource utilization [33,34], solar rays are another power source that should be considered. A solar concentrator, also known as linear Fresnel mirrors (LFRs), is a device that can be utilized to transform solar power into a thermal form. Numerous pieces of research have shown that LFRs are indeed a viable and appropriate option that may fulfill current energy requirements [35,36].

HNFs are really a viable option for raising the temperature quality of either the experimental liquid by maximizing the thermal transition capability [37–45]. Because LFR has low thermal effectiveness, HNFs are a solution to the problem of something like the LFR's poor thermal usefulness.

The ability of any material to conduct heat is called thermal conductivity. Thermal conductivity varies from material to material copper and aluminum possess high thermal conductivity in contrast to other materials. In fluids, thermal conductivity occurs due to the intermolecular collision of atoms of the fluid. The term "thermal conductivity" describes how quickly heat moves among atoms. A fluid with such a high thermal conductivity will heat up or cool down more quickly compared to one that has low thermal conductivity. Thermal conductivity is widely used in computer applications like cooling of CPUs, GPUs, and some chipsets and RAM modules. Thermal conductivity analyzers offer quick and simple ways for monitoring heat transfer fluids in the automotive, industrial, and aerospace industries. Researchers across the world investigated the effect of thermal conductivity on fluids containing high thermal conductivity nanoparticles to investigate heat transfer analysis. Algehyne et al. [46] investigated the influence of ternary hybrid nanoparticles on pseudoplastic fluid flow subjected to an expandable sheet accompanied by Fourier's heat flux and variable thermal conductivity.

THNF with the utilization of Buongiorno tri hybrid nanofluid on Prandtl fluid moving towards a wedge accompanied with activation energy as well as thermal were investigated in detail by Sajid et al. [47]. Wang et al. [48] adopted Galerkin finite element scheme in order to achieve the numerical solution of ternary hybrid nanofluid comprising distinguished effects like variable diffusivity, thermal conductivity, and Cattaneo-Christov heat flux. Sajid et al. [49] adopted tetra hybrid nanoparticles on Reiner-Philippoff fluid and further tackled this model numerically with Galerkin finite element scheme.

Through the exploitation of tetra HNFS (SiO_2, TiO_4, Cu, Al_2O_3/EG), the purpose of this research will be to conduct a study in terms of the heat transport mechanism of a solar automobile. The extendable plate, as in a solar array, will serve as the focal point of this investigation. Radiation from the sun has indeed been taken into consideration as a potential source of heat. The functionality of a renewable energy car's heat transport mechanism is examined for such a scenario of many effects, such as thermal radiated flux, heat production, and variable thermal admittance. To handle modelled momentum and energy equations, the Cash and Carp approach is used. This procedure was given its name since it was developed by Cash and Carp. The effects of a wide variety of factors on temperatures and velocity fields, together with the surface drag coefficient and heat transmission rate, were extensively described and illustrated in the form of tables as well as figures.

1.1. Modeling purpose

The automotive industry on every continent has been working hard to improve the thermal efficiency of solar-powered vehicles by using a wide variety of different strategies. The present study is set up in such a way that it can investigate the heat transference characteristics of solar vehicles via the use of tetrahybrid nanofluid that is driven past solar plates that are mounted on the top of solar cars. Solar radiation has been taken into consideration as a potential source of heat. The efficiency computation of a solar car's heat transfer system is being evaluated concerning several potential consequences, including thermal radiations, changing thermal conductivity, and viscous dissipation.

1.2. Novelty

The paper is original in the respect that now the influence of a unique and creative tetrahybrid nanofluid especially in the case of modified tetrahybrid Hamilton and Crosser model in the case of novel binary fluid having the combination of Casson fluid as well as Sutterby fluid flow that is exposed to a solar sheet has still not been explored throughout the current literature. This means that the impact of the article will be the first of its kind.

1.3. Mechanism of a solar-powered car

1.3.1. Solar panel

Solar radiations are one of the most powerful mechanisms of solar energy. Solar radiations directly coming from the sun fall on the surface of the solar panel. The stretching sheet is located inside the solar panel. Tetra hybrid nanofluid is flowing over a stretching sheet. Solar radiations penetrated through the solar panel sheet and fell on the stretching sheet. The capacity of the solar panel is effectively increased to absorb solar radiation due to the presence of tetra-hybrid nanoparticles.

1.3.2. Power tracker

From the solar panel, the stored energy is delivered to the power tracker. Power point tracking is a strong DC-to-DC inverter that serves as the ideal electrical load for a solar array and transforms the power into a current. In the absence of a power tracker, the DC motor would perform badly.

1.3.3. Battery Pack

Electric cars, as readers probably already know, rely on electricity rather than fuel and accumulate power in their onboard backup batteries to be utilized at a later time. A battery is what stores the energy for subsequent use. The photovoltaic system powers the battery, which then turns solar power into electrical power. As a result, the longer you allow the battery of your automobile to recharge during daylight hours (when it is exposed to sunlight), the fewer problems you will encounter while driving at night. This energy in terms of electricity is used in solar vehicles in order to facilitate navigation.

1.3.4. Motor controller

Both DC voltage and alternating current motors employ motor regulators. A regulator contains a way to attach the motor to the source of electrical power. It could also contain overload and above current safety for the wiring as well as motor safety. Additionally, a

motor controller may monitor the motor's peripheral circuit or look for issues like poor deliverance of voltage.

In traditional automobiles, the engines are replaced by electric motors. The motor is very effective at transforming electrical energy into the mechanical energy required to move the vehicle and its unique design is that it has been positioned inside the wheels. This maintains a high level of performance (Fig. 1(a)).

2. Mathematical formulation

Fig. 1(b) is intended to be used for research into the process of heat exchange analysis conducted on the solar vehicle. Solar rays penetrate the solar array and land on its surface. Within the photovoltaic panels themselves, you will find the expanding surface sheet. Radiation could pass through a sheet used for photovoltaic panels and disperse on another sheet used for expanding. SiO_2 TiO_2, Cu, Al_2O_3/EG kind tetra hybrid nanoliquid is flowing across the sheet as it spans down along the x-axis. The liquid known as ethylene glycol is classified as a foundation liquid. The temperature variation within the solar vehicle is amplified owing to the movement of tetra hybrid nanoliquid across a flexible layer, along with the effects of solar radiation. In order to evaluate the thermal transport efficiency of an expandable sheet and then a solar vehicle, a number of factors, including changing conduction due to thermal phenomena, thermal types of radiation, and heat production, were taken into consideration. The T_w and T_∞ stand again for the temperature of the wall as well as the free stream, respectively. The dynamical viscidity, consistency, thermal conductivity, and thermal conductance of a tetra hybrid nanofluid are shown by the μ_{tethnf}, ρ_{tethnf}, k_{tethnf} and $(C_p)_{tethnf}$ variables, respectively (TETHNF).

2.1. Limitations of the present model and its scientific implementations

- Mixed Casson Sutterby fluid is considered along with a porous expandable sheet. Fluid flow through a porous media has many industrial applications such as water flowing through rocks and soil and purification of gas and oil mixed in rocks.
- Incompressible fluid is considered whose density does not vary with pressure.
- The assumption of laminar flow is made. In the momentum equation indicated in (2), the diffusive phenomenon wins over the convective phenomenon. Solar vehicles, airplanes, engineers, and even scientists all benefit from laminar flow's unique properties. Although the losses due to friction remain lower in laminar flow, it is far more effective than turbulent flow. Since there is no turbulence or disorder in laminar flow, it is much quieter than turbulent flow. This is particularly helpful in noisy situations, including aircraft, submarines, and certain types of plumbing.
- The mathematical model takes tetra nanoparticles into account to study the heat transfer phenomena. Tetra nanoparticles have a significant effect on the design of the solar car's exterior, solar panels, interior, etc. The heat transfer phenomenon is amplified when agglomerative nanoparticles are introduced into the base fluid. Nanoparticles made of materials like titanium, copper, and aluminum are also rather lightweight. Titanium alloys with higher specific strengths than pure titanium are utilized in the construction of solar vehicles' body structures because of their low weight, high strength (high specific strength), and great heat resistance. Copper is used extensively in solar cars, from batteries and inverters to wiring and solar panels at charging stations. Copper's versatility is due to the combination of its physical qualities, including its strength, conductivity, corrosion resistance, machinability, and ductility. Aluminum is of interest to many solar energy firms because of its unique qualities. Inseparable from solar power systems due to its lightweight, high strength, suitable corrosion characteristics, high surface reflectivity, outstanding electrical and thermal conductivities, and specific optic qualities of its anodic coating.

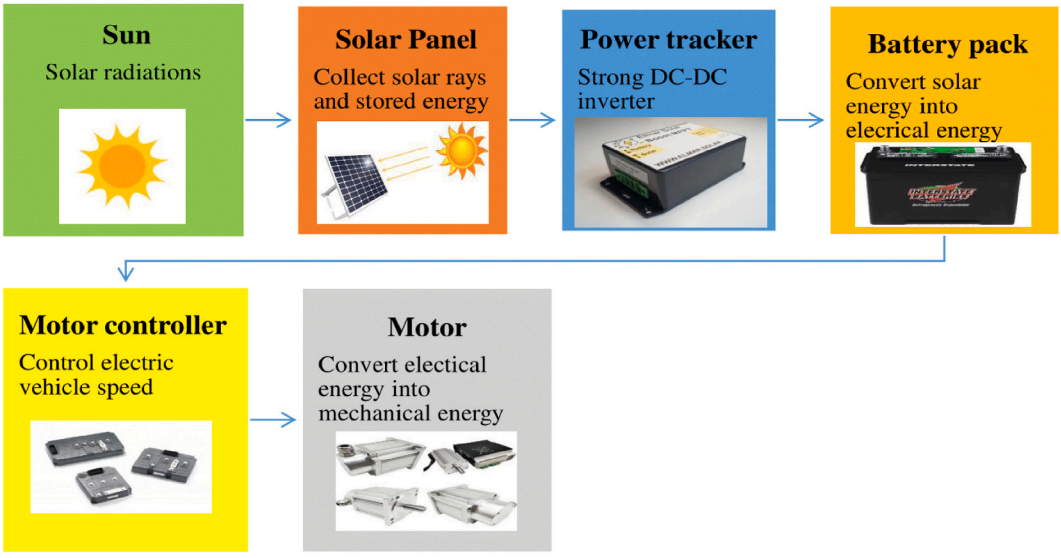

Fig. 1(a). Working of solar power car.

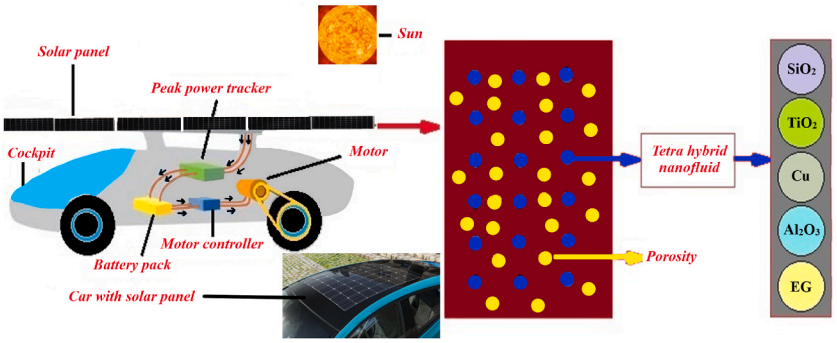

Fig. 1(b). Schematic display of the solar-powered car.

- The energy equation takes into account the phenomena of thermal radiation, thermal conductivity variability, and heat creation. The thermal conductivity of the base fluid is greatly improved by the use of tetra-hybrid nanoparticles. In this investigation, strong heat conductivity was required, and tetra-hybrid nanoparticles were delivered. Nanoparticles are employed in the fabrication of solar panel sheets to increase the amount of energy drawn from the sun and stored in the battery under low-light conditions. For this reason, scientific consensus favors solar panels whose alloys have copper, aluminum, titanium, and silica nanoparticles. The energy we get from the sun is infinite and clean. In this case, the source of the thermal radiation is understood to be the sun's emitted electromagnetic waves. Solar-powered vehicles, airplanes, streetlights, windmills, and other devices may all harness the sun's rays and convert them into useable heat and electricity.
- The mathematical model, which includes momentum and energy equations, has distinguished scientific applications in the design of solar-powered cars, solar-powered aircraft, nuclear reactors, the design of airfoils, the production of polymers, solar sheets, etc., because it takes into account effects such as porosity, nanoparticles, thermal conductivity, thermal radiation, and heat generation.

The controlling modelled equations [50–52] are given by

$$\frac{\partial u}{\partial x}+\frac{\partial v}{\partial y}=0, \tag{1}$$

$$u\frac{\partial u}{\partial x}+v\frac{\partial u}{\partial y}=\frac{1}{2}\frac{\mu_{tethnf}}{\rho_{tethnf}}\frac{\partial}{\partial y}\left[\left(1+\frac{1}{\beta}\right)\frac{\partial u}{\partial y}-\frac{MB^2}{2}\left(\frac{\partial u}{\partial y}\right)^2\right]-\frac{\mu_{tethnf}}{\rho_{tethnf}K}u, \tag{2}$$

$$u\frac{\partial T}{\partial x}+v\frac{\partial T}{\partial y}=\frac{\partial}{\partial y}\left(\frac{k_{tethnf}}{(\rho C_p)_{tethnf}}\frac{\partial T}{\partial y}\right)-\frac{1}{(\rho C_p)_{tethnf}}\frac{\partial q_r}{\partial y}+\frac{Q_0(T-T_\infty)}{(\rho C_p)_{tethnf}}, \tag{3}$$

The associated boundary constraints are:

$$\left.\begin{array}{l} y=0: u=ax, v=0, T=T_w, \\ y\to\infty: u\to 0, T\to T_\infty. \end{array}\right\} \tag{4}$$

TETHNF Hamilton and Crosser nanofluid model are bestowed by Refs. [27,28]:

$$\left.\begin{array}{l} \mu_{tethnf}=\dfrac{\mu_f}{(1-\varphi_1)^{2.5}(1-\varphi_2)^{2.5}(1-\varphi_3)^{2.5}(1-\varphi_4)^{2.5}}, \\ \rho_{tethnf}=\left[(1-\varphi_1)\left\{(1-\varphi_2)(1-\varphi_3)\left[(1-\varphi_4)\rho_f+\rho_4\varphi_4\right]+\rho_3\varphi_3+\rho_2\varphi_2\right\}+\rho_1\varphi_1\right], \\ (\rho C_p)_{tethnf}=(1-\varphi_1)\left\{(1-\varphi_2)(1-\varphi_3)\left[(1-\varphi_4)(\rho C_p)_f+(\rho C_p)_{s_4}\varphi_4\right]+(\rho C_p)_{s_3}\varphi_3+(\rho C_p)_{s_2}\varphi_2\right\}+(\rho C_p)_{s_1}\varphi_1, \\ \dfrac{k_{tethnf}}{k_{thnf}}=\dfrac{k_4+k_{thnf}(n-1)-(1-n)\varphi_4(k_4-k_{thnf})}{k_4+(n-1)k_{thnf}+\varphi_4(k_{thnf}-k_4)}, \dfrac{k_{thnf}}{k_{hnf}}=\dfrac{k_3+k_{hnf}(n-1)-(1-n)\varphi_3(k_3-k_{hnf})}{k_3+(n-1)k_{hnf}+\varphi_3(k_{hnf}-k_3)}, \\ \dfrac{k_{hnf}}{k_{nf}}=\dfrac{k_2+k_{nf}(n-1)-(1-n)\varphi_2(k_2-k_{nf})}{k_2+(n-1)k_{nf}+\varphi_2(k_{nf}-k_2)}, \dfrac{k_{nf}}{k_f}=\dfrac{k_1+k_f(n-1)-(1-n)\varphi_1(k_1-k_f)}{k_1+(n-1)k_f+\varphi_1(k_f-k_1)}. \end{array}\right\} \tag{5}$$

Thermophysical properties of SiO_2 TiO_2, Cu, and Al_2O_3 nanoparticles on EG as shown in Table 1.
The expression regarding Rosseland approximation and variable thermal conductivity is bestowed by

$$k_{tethnf}(T)=k_{tethnf}(1+\varepsilon\theta) \tag{6}$$

$$q_r=-\frac{4\sigma^*}{3\kappa^*}\frac{\partial T^4}{\partial y}, \tag{7}$$

Table 1
Thermophysical properties [8,15,24,47,50].

Properties	EG	SiO_2	TiO_2	Cu	Al_2O_3
ρ	1114	3970	4250	8933	3970
C_p	2415	765	690	385	765
k	0.252	36	8.953	400	40

while σ^* and κ^*, which are relative to one another, indicate the Boltzmann factor and the absorption factor, accordingly.

Afterward, take into consideration the appropriate similarity variables adjustment that was listed down below.

$$u = axf^{'}(\eta), v = -\sqrt{av}f(\eta), \eta = \sqrt{\frac{a}{\nu}}y, \theta(\eta) = \frac{T - T_\infty}{T_w - T_\infty}. \tag{8}$$

Transformed Eqs. (2)–(5) in the light above similarity variables are

$$\left[\left(1+\frac{1}{\beta}\right) - \frac{M}{2}ReDef''^2\right]f''' + 2A_1A_2ff'' - 2A_1A_2f'^2 - 2\lambda f' = 0, \tag{9}$$

$$\left\{\left[\left((1+\varepsilon)+\frac{Rd}{A_4}\right)\theta'' + \varepsilon\theta'^2\right]\right\} + \frac{2}{3}\frac{A_3}{A_4}Prf\theta' + \frac{Q}{A_4}\theta = 0, \tag{10}$$

Respective BCS (6) are

$$\left.\begin{array}{l} \eta = 0 : f(\eta) = 0, f'(\eta) = 1, \theta'(0) = 1, \\ \eta \to \infty : f'(\eta) \to 0, \theta(\eta) \to 0. \end{array}\right\} \tag{11}$$

Dimensionless quantities are enumerated underneath:

$$\left.\begin{array}{l} De = \dfrac{B^2a^2}{\nu},\ Pr = \dfrac{\mu C_p}{k_\infty},\ Rd = \dfrac{16\sigma T_\infty^3}{3k^*k_\infty},\ \lambda = \dfrac{\nu}{aK}, \\ Re = \dfrac{u_w x}{\nu},\ Q = \dfrac{Q_0(T_0 - T_\infty)}{(\rho C_p)_{hnf}}. \end{array}\right\} \tag{12}$$

The rate of heat transfer and the drag on the surface both contributed

$$Cf_x = \frac{\tau_w}{\rho u_w^2}, Nu_x = \frac{xq_w}{k_f(T_w - T_\infty)}, \tag{13}$$

although the shear rate, designated by τ_w, the wall temperature gradient, denoted by q_w mentioned below

$$\tau_w = -\mu_{tethnf}\left[\left(1+\frac{1}{\beta}\right)\frac{\partial u}{\partial y} + \frac{MB^2}{3}\left(\frac{\partial u}{\partial y}\right)^3\right], q_w = -\left[k_{tethnf} + \frac{16\sigma^*}{3\kappa^*}T_\infty^3\frac{\partial T}{\partial y}\right]. \tag{14}$$

There is also a dimensionless variant of surface drag, which is illustrated by

$$Cf_xRe_x^{1/2} = -\frac{1}{A_1}\left[\left(1+\frac{1}{\beta}\right)f'' + \frac{M}{3}ReDef''^3\right], \tag{15}$$

Proper attribution of the non-dimensional heat transition rate lies with

$$Nu_xRe_x^{-1/2} = -A_4(1+Rd)\theta' \tag{16}$$

whereas A_1, A_2, A_3, A_4 are given by

$$\left.\begin{array}{l} A_1 = (1-\varphi_1)^{-2.5}(1-\varphi_2)^{-2.5}(1-\varphi_3)^{-2.5}(1-\varphi_4)^{-2.5}, \\ A_2 = (1-\varphi_1)\left\{(1-\varphi_2)(1-\varphi_3)\left[(1-\varphi_4) + \varphi_4\dfrac{\rho_4}{\rho_f}\right] + \varphi_3\dfrac{\rho_3}{\rho_f} + \varphi_2\dfrac{\rho_2}{\rho_f}\right\} + \varphi_1\dfrac{\rho_1}{\rho_f}, \\ A_3 = (1-\varphi_1)\left\{(1-\varphi_2)(1-\varphi_3)\left[(1-\varphi_4) + \dfrac{(\rho C_p)_{s_4}}{(\rho C_p)_f}\varphi_4\right] + \dfrac{(\rho C_p)_{s_3}}{(\rho C_p)_f}\varphi_3 + \dfrac{(\rho C_p)_{s_2}}{(\rho C_p)_f}\varphi_2\right\} + \\ \dfrac{(\rho C_p)_{s_1}}{(\rho C_p)_f}\varphi_1, \\ A_4 = \dfrac{k_{tethnf}}{k_f} \end{array}\right\} \tag{17}$$

Table 2 presents a resemblance of the mathematically produced results with those found in Waini et al. [52] with and without nanoparticles*Rd*.

3. Solution methodology

The Cash and Carp method (11) is used to solve equations (9) and (10), which, when put together with endpoint constraints (11), make up the modelled problem. Due to the fact that Cash and Carp seem to have a rounding error having order 5, influences results more favorably than even a variety of those other approaches (see Table 1). Equation (9) through (10) are complex in their behavior and solving them analytically is indeed an extremely time-consuming endeavor due to the complexity of the problem. The final objective would be to perform numerical analysis on the system of equations while taking into account BCS (11). There are a number of different numerical approaches that have been employed to solve these sorts of equations, and we are able to solve equations by using our shooting skills in conjunction with the RKF approach. Literally, the entire process is often referred to as the "Cash and Carp" technique. The equations can be transformed into BVP problems by assigning symbols to miss starting conditions, and once this is done, the shooting approach, along with RKF, can be used successfully in BVP. Partial differential equations have been converted into first-order ODEs, which represent.

$$f = z_1, f' = z_2, f'' = z_3, \theta = z_4, \theta' = z_5, \tag{18}$$

First-order ODEs are given by

$$z_3{}' = \frac{2\lambda z_2 + 2A_1A_2{z_2}^2 - 2A_1A_2z_1z_3}{\left(\left(1+\frac{1}{\beta}\right) - \frac{M}{2}ReDe\ {z_3}^2\right)}, \tag{19}$$

$$\left\{\left[(1+\varepsilon)+\frac{Rd}{A_4}\right]z_5{}' + \varepsilon\ {z_5}^2\right\} + \frac{A_3}{A_4}Pr\ z_1z_5 + \frac{Q}{A_4}z_4 = 0, \tag{20}$$

BCs (6) are now

$$\left.\begin{array}{l} \eta = 0 : z_1(\eta) = 0, z_2(\eta) = 1, z_5(0) = 1, \\ \eta \to \infty : z_5(\eta) \to 0, z_4(\eta) \to 0. \end{array}\right\} \tag{21}$$

The RKF of the fourth and fifth orders is used to figure out how to solve the above ODEs.

$$\left.\begin{array}{l} \mathbf{K_1} = h\mathbf{F}(\eta, \mathbf{Z}), \\ \mathbf{K_i} = h\mathbf{F}\left(\eta + A_i, \mathbf{Z} + \sum_{j=1}^{i-1} B_{ij}\mathbf{K_j}\right), i = 2, 3, ..., 6, \\ \mathbf{Z_5}(\eta + h) = \mathbf{Z}(\eta) + \sum_{i=1}^{6} C_i\mathbf{K_i}, \\ \mathbf{Z_4}(\eta + h) = \mathbf{Z}(\eta) + \sum_{i=1}^{6} D_i\mathbf{K_i}, \end{array}\right\} \tag{22}$$

where the formulae of the fourth as well as fifth orders are indicated by indices 4 but also 5, respectively. In turn, $\mathbf{K_1}$, $\mathbf{K_i}$, $\mathbf{F}$ and $\mathbf{Z}$ are almost all classified as

$$\mathbf{K_1} = \begin{bmatrix} K_{11} \\ K_{12} \\ K_{13} \\ K_{14} \\ K_{15} \end{bmatrix}, \mathbf{K_i} = \begin{bmatrix} K_{i1} \\ K_{i2} \\ K_{i3} \\ K_{i4} \\ K_{i5} \end{bmatrix}, \mathbf{F} = \begin{bmatrix} f_{11} \\ f_{12} \\ f_{13} \\ f_{14} \\ f_{15} \end{bmatrix}, \mathbf{Z} = \begin{bmatrix} z_{11} \\ z_{12} \\ z_{13} \\ z_{14} \\ z_{15} \end{bmatrix} \tag{23}$$

in which $i = 2, 3, ...6$. The coefficients in the RKF formula are enumerated underneath in Table 3.

The problem-solving process requires careful consideration of the path length h that is used. In the context of the current issue, the measurement of h is defined as 0.1. equations 19–21 may be numerically investigated by using the method for such a fifth order. The procedure for the fourth order can only be employed for the truncation error reasons described further down.

Table 2
In light of Ref. [52], a comparison of the present numerical consequences.

$Nu_xRe_x^{\frac{-1}{2}}$ (Absent *De*, λ *and Q*)		
	$\beta \to \infty$, $Pr = 2$	
Rd	Current	Waini et al. [52]
0.0	0.764374	0.764357
1.0	0.443323	0.443323

$$E(h) = Z_5(\eta + h) - Z_4(\eta + h) = \sum_i (C_i - D_i)K_i \tag{24}$$

The term "residual" refers to the disparity that exists between numbers that have been numerically calculated and boundary values. The ultimate answer has been attained whenever the variance between the residuals at the boundary is smaller than the tolerance threshold of 10^{-6} in order to enhance the initial limitations that were absent. The iterative method developed by Newton is used. The following are the criteria that will determine whether the iterative process is complete:

$$\max\{|z_2(\eta_{max}) - 0|, |z_4(\eta_{max}) - 0|, |z_6(\eta_{max}) - 0|\} < 10^{-8} \tag{25}$$

Table 3 provides an illustration of the coefficients that are used in the RKF technique. The coefficients are listed below.

In an attempt to show that the mathematical technique is accurate, we matched current findings with those obtained previously by Reddy et al. [52] with missing *Rd* but also discovered that there was a great agreement among the two sets of data.

4. Results and discussions

The goal would be to investigate the impact of a variety of non-dimensional factors on the velocity distribution $f'(\eta)$ and by extension, the temperature distribution $\theta(\eta)$. The significance of a number of non-dimensional factors in terms of heat transmission study for such a scenario of an extended sheet located within the photovoltaic array panels of such a hybrid electric vehicle has been investigated, and the results have been communicated in the form of tables and graphs.

Fig. 2(a) sketched the influence of Casson fluid parameter β on $f'(\eta)$. The fluid behaves like shear thinning in the case of $\beta > 1$. The liquid viscosity decreases as a result of an increase in β, which also contributes to a reduction in the velocity of the fluid. Both of these factors lead to the minimizing of the fluid's viscosity. The liquid becomes more viscous by improving β debacles velocity of fluid moving over an expandable sheet located inside the solar panel surface sheet. Physically a fluid exhibits large viscosity and provides resistance to fluid motion moreover strong bond between intermolecular forces provides it with a lot of internal friction, resisting the movement of layers flow over one another and lessening the fluid velocity $f'(\eta)$. Impact of Sutterby fluid viscosity ratio parameter M on $f'(\eta)$ is highlighted in Fig. 2(b). The behavior of parameter M is similar to Casson fluid parameter β. It is noted that the fluid behavior is shear thickening in the case of $M < 0$, $M = 0$ Newtonian fluid in addition to shear thickening for $M > 0$. Casson Sutterby fluid is a viscoelastic fluid having viscosity changes over time. Daily life products having viscosity changes over time are ketchup, paint, blood, spaghetti, polymers, etc. Viscosity is the key factor responsible for a decrement in fluid velocity. A tight intermolecular bond resists the fluid flow. Physically speed of a fluid decreases as its viscosity improves This is due to the two different sloping planes upon which you pour the honey and water. You'll realize that honey has a greater degree of viscosity than water, which causes it to move along the inclined surface at a slow speed. Thus, we are now able to claim that velocity seems to decline as the viscosity grows. From Fig. 2(b) it is observed that the fluid behavior is shear thickening by amplifying TETHNF agglomeration in base liquid.

The impact of Reynolds's number and Deborah's number of velocity fields are highlighted in Fig. 2(c) and Fig. 2(d) respectively. Both factors are reliable on the viscosity of the fluid flow. Viscous forces dominate in the case of smaller Reynold's number. It is observed that fluid behavior is laminar, and the viscosity of the fluid amplifies. Insertion of nanoparticles in the base fluid amplifies liquid density and is denser by adding TETHNF in contrast to TEHNF. Reynolds number is defined as inertial forces to viscous forces. Physically "weak flow energy" loses the battle against "viscous forces (sticky forces)" that try to stop the fluid from moving, the lower the Reynolds number, the fewer "inertial forces" are fighting in order to keep the fluid running. As a result, the velocity field diminishes as shown in Fig. 2(c). Deborah's number is the ratio of the relaxation time of the fluid to the experimental time. It is a crystal clear liquid that changes from liquid to solid by virtue of magnification in *De*. The mixture of corn starch and liquid is the best example of this phenomenon having viscosity changes over time and fluid changes from liquid to solid. For higher Deborah numbers (De), the viscous consequences become more pronounced physically. These slow down the flow over the whole domain, causing a smaller momentum barrier layer. Since *De* distinguishes between solids and liquids (or fluids), an object with a low De acts as a liquid, while a substance with a high *De* responds as a viscoelastic solid, such as rubber, jelly, polymers, etc. It is quite that liquid viscosity amplifies for $De < 1$ which lessens the liquid motion (Fig. 2(d)). With increasing levels of volume proportion of nanofluid, the fluid velocity decreases. By adding nanoparticles, the fluid will essentially be becoming more sluggish, which will enhance the Casson-Sutterby fluid viscosity.

Fig. 3(a) reflects the impact of thermal conductance ε on $\theta(\eta)$. It is well established that TBL layer thickness amplifies more for TETHNF in contrast to TEHNF as shown in the figure. The stretching sheet located inside the solar panel sheet distributes incremental heat by amplifying ε which improves the heat distribution system in the solar hybrid vehicle. The physical ability of a material to conduct heat amplifies under magnification in ε. It is well-established that molecules collide more randomly and share more kinetic

Table 3
The arithmetic representations of the indices provided by Cash and Carp.

i	A_i			B_{ij}			C_i	D_i
1	–	–	–	–	–	–	37/378	2825/27648
2	1/5	1/5	–	–	–	–	0	0
3	3/10	3/40	9/40	–	–	–	250/621	18 575/48384
4	3/5	3/10	9/40	6/5	–	–	125/594	13 525/55296
5	1	11/54	5/2	70/27	35/27	–	0	277/14336
6	7/8	1631/55296	175/512	575/13824	44275/110592	253/4096	512/1771	1/4

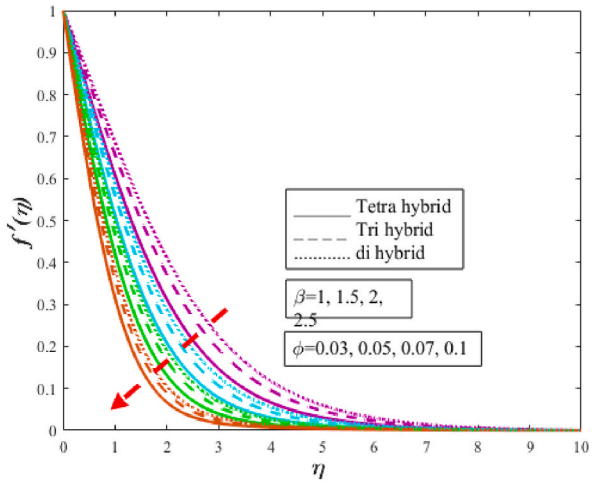

Fig. 2(a). Impression of Casson fluid parameter β on $f'(\eta)$.

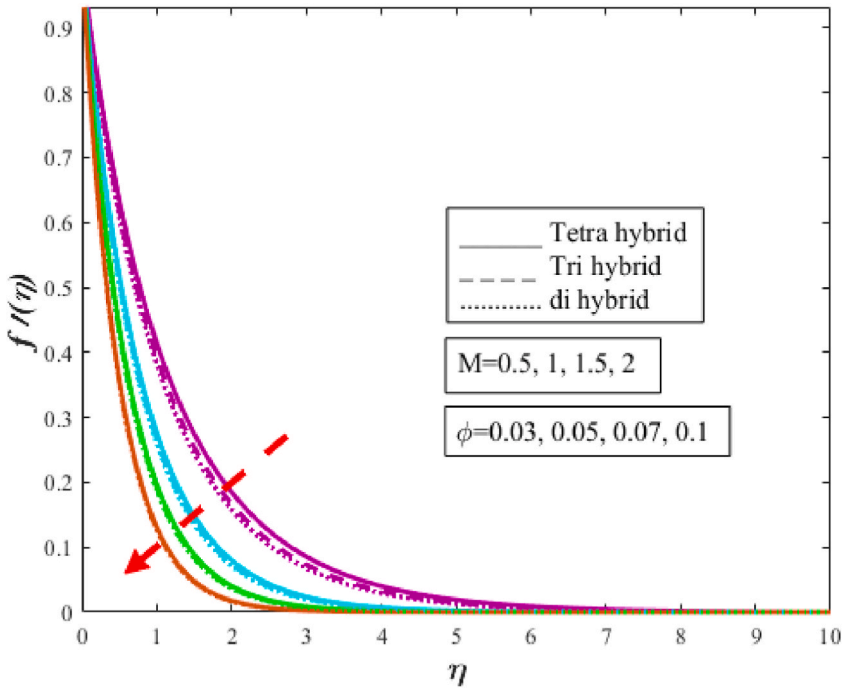

Fig. 2(b). Impression of Sutterby fluid viscosity parameter M on $f'(\eta)$.

energy with each other by improving ε which amplifies $\theta(\eta)$. Insertion of nanoparticles in the base fluid also amplifies heat transfer rate and ε. Fig. 3(b) reflects *Pr* impact on $\theta(\eta)$. Prandtl is momentum diffusivity to thermal diffusivity. Diffusivity in the case of momentum dominates thermal diffusivity in the case of thermal transport which lessens temperature. Physically heat diffuses more quickly by improving Pr and amplifies more for TETHNF to TEHNF. As a result, $\theta(\eta)$ diminishes. The effect of Q as well as Rd against $\theta(\eta)$ are highlighted in Fig. 3(c) and (d). Physically heat generation phenomenon works on the principle of an exothermic reaction. During exothermic reactions, energy is released in the form of light or heat. Physically heat is released to the environment, resulting in an improvement in the overall temperature of the fluid which eventually amplifies the heat transport rate of the fluid and $\theta(\eta)$. When nanoparticles are added to base fluid, more radiation is absorbed than when plain fluid is used. Thermal radiations are actually electromagnetic waves that penetrated through the fluid. Actually, thermal radiation is used in situations where a lot of heat is needed. Rising Rd increases the amount of heat transfered to a system, amplifying the temperature inside the fluid and ultimately amplifying $\theta(\eta)$. Thermal boundary thickness as well as heat transfer in terms of TETHNF is more rather than TEHNF. More heat is transfered by rising Q furthermore amplifying the heat transfer phenomenon. Whenever sun rays hit a solar panel, which itself is positioned on the

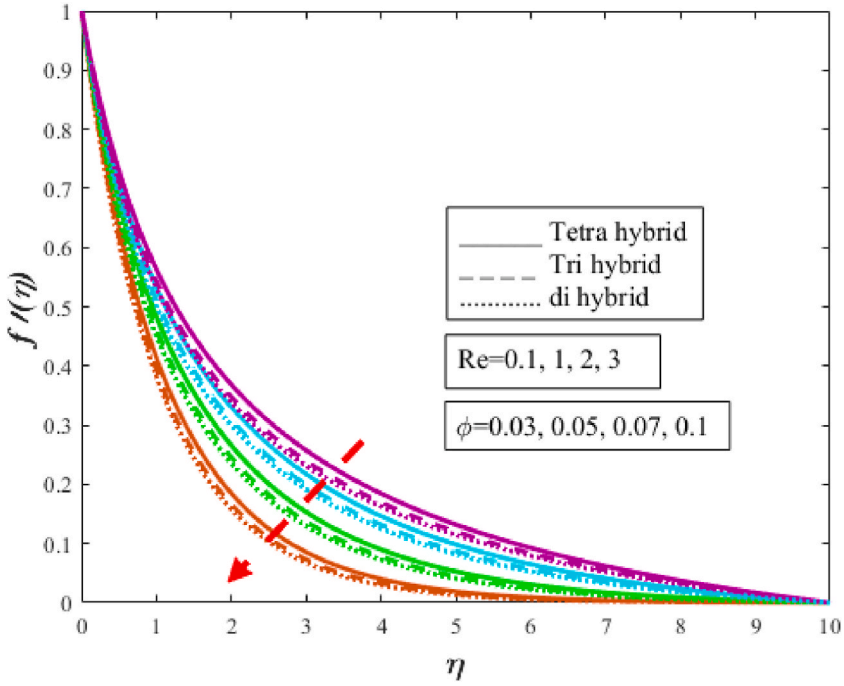

Fig. 2(c). Impression of Reynolds number *Re* on $f'(\eta)$.

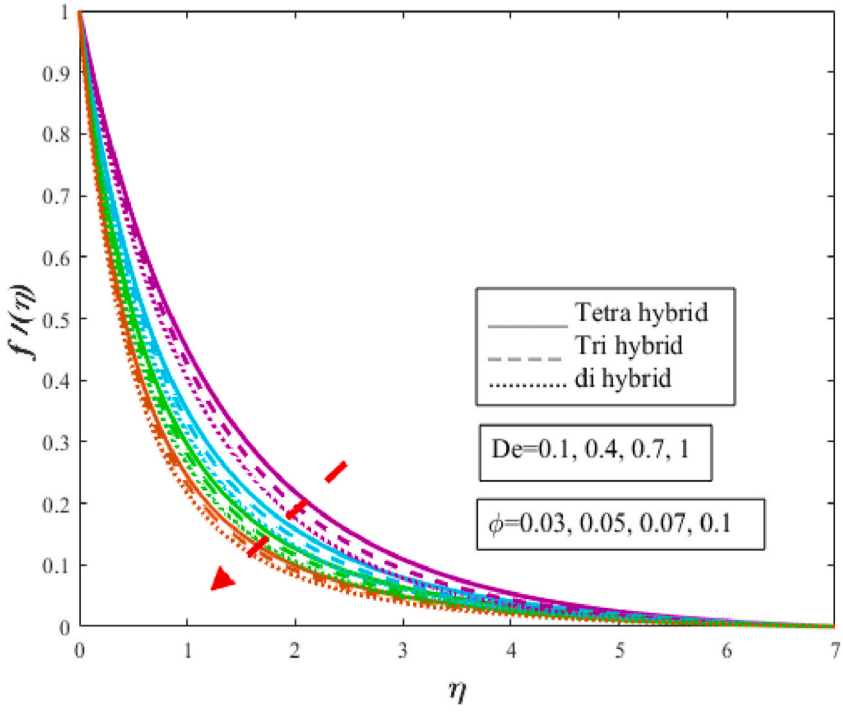

Fig. 2(d). Impression of Deborah number *De* on $f'(\eta)$.

topmost rooftop of something like a renewable vehicle, this is known as "solar absorption." The stretched sheet that is positioned within the photovoltaic array panel sheet has the capability of increasing its interior thermodynamic efficiency, which in turn gives substantial heat to such nanostructured liquids. In comparison to the situation of conventional liquids, the heat is transfered more efficiently in the case of a TETHNF-based liquid. The primary contributor to the generation of heat energy is radiation. Solar thermal types

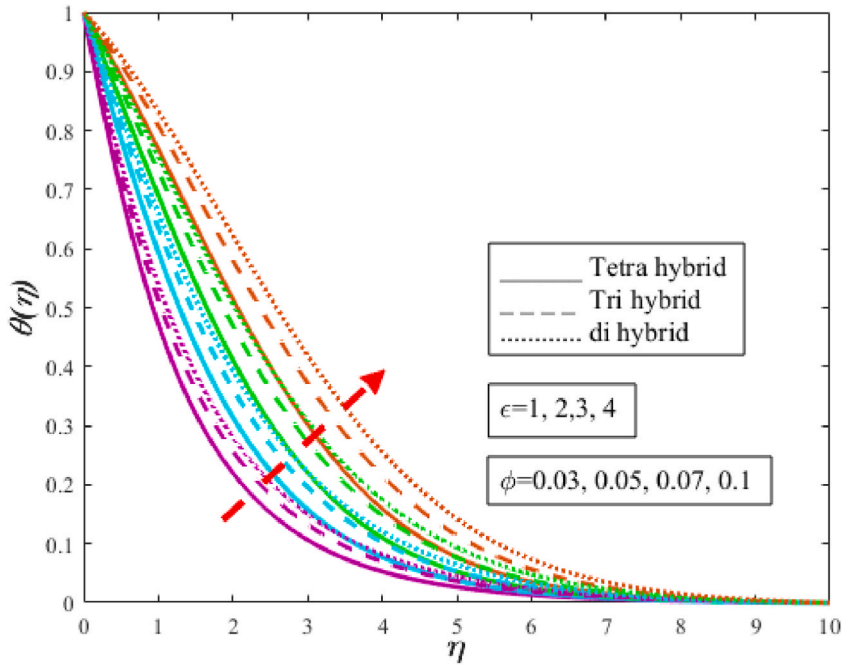

Fig. 3(a). Impact of thermal conductivity ε on $\theta(\eta)$.

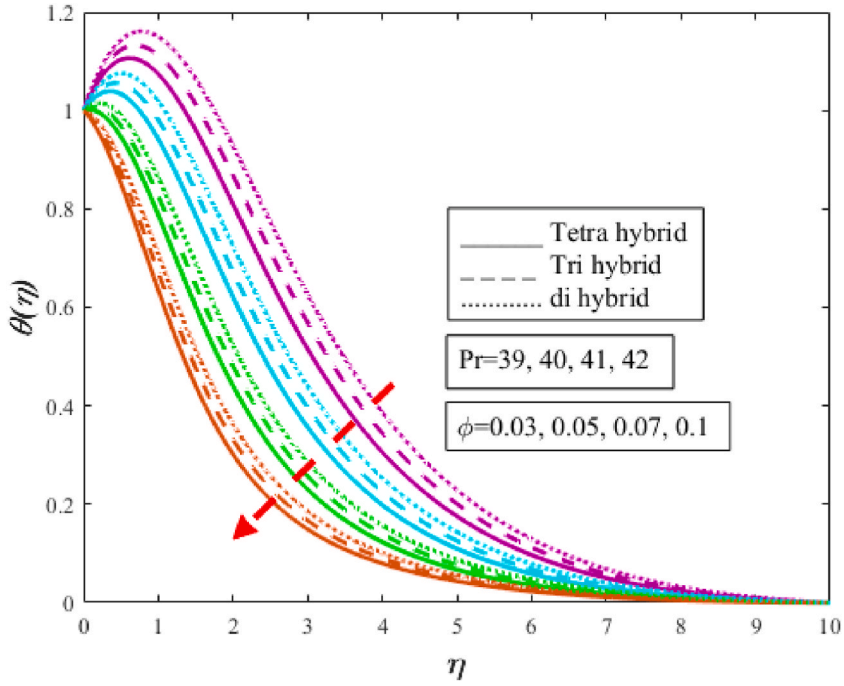

Fig. 3(b). Impact of Prandtl number *Pr* on $\theta(\eta)$.

of radiation have already caused a fundamental shift in our understanding of sustainable power and have also inspired academics to pursue novel avenues of inquiry into the development of solar-powered vehicles, photovoltaic aircraft wings, solar pumping stations, solar scooters, and other such technologies. The ability to store energy is among the most important aspects of how a solar vehicle operates. The use of nanoparticles, as well as the use of such a beneficial base liquid, are critical characteristics that must be used to improve the efficacy of natural sunlight rays falling on the stretched sheet that is positioned inside the solar array sheet. Solar radiations consistently land somewhat on the plane of such an extending medium, transferring a significant amount of heat to TETHNF

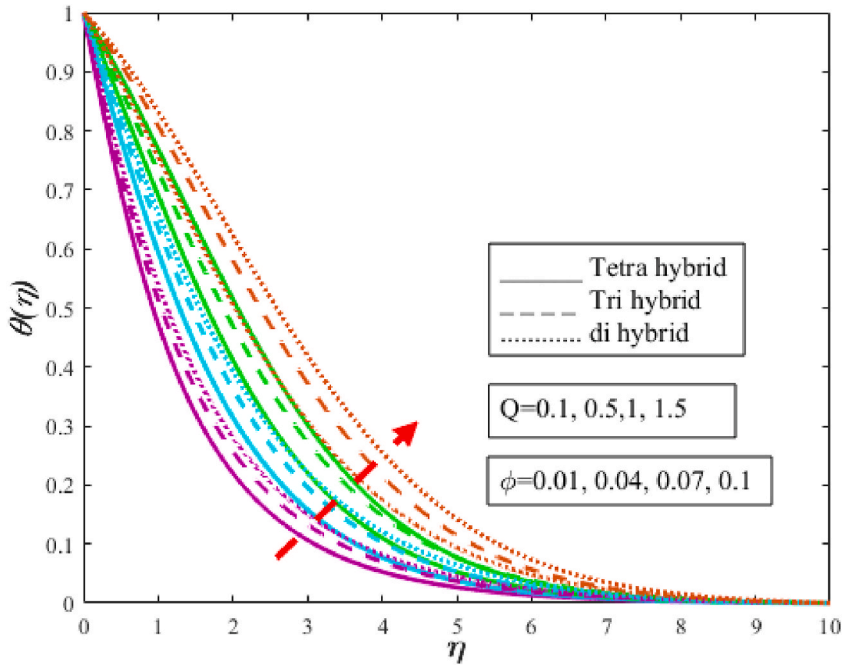

Fig. 3(c). Impact of heat generation Q on $\theta(\eta)$.

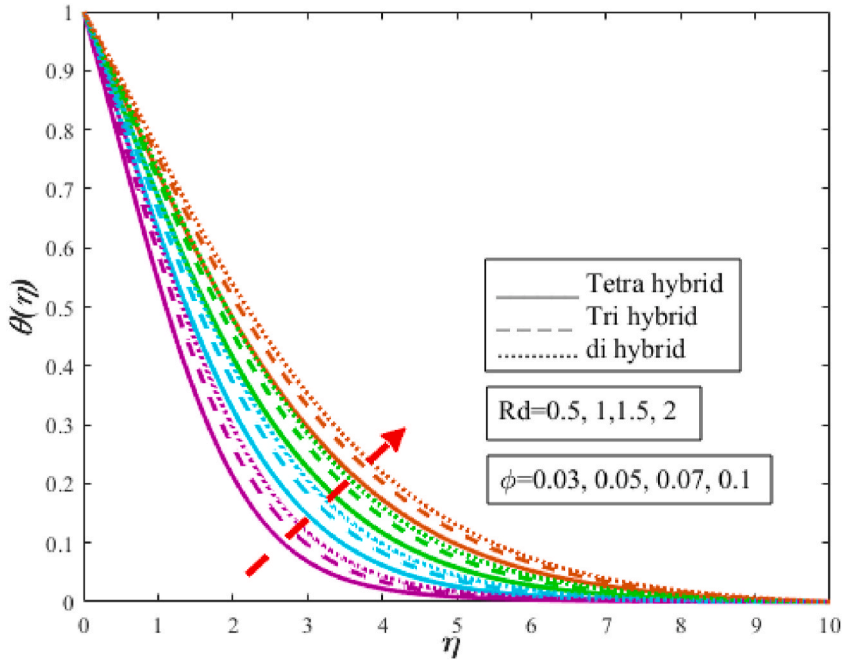

Fig. 3(d). Impact of thermal radiation parameter Rd on $\theta(\eta)$.

flowing across the expandable sheet that is positioned within the solar photovoltaic array. Throughout the event that Rd is magnified, the heat conduction mechanism of something like the liquid will strengthen, which will also increase the heat phenomenon. Because *Rd* and *Q*, which measure the rate of heat creation, have increased, the temperature and total rate of heat transference have improved.

In Table 4, the influence of ε, *Pr*, *Ec*, *Q*, and *Rd* on heat transfer was outlined for the cases TETHNF SiO_2 TiO_2, Cu, Al_2O_3/EG as well as SiO_2 TiO_2, Cu/EG. Concerning the rate at which heat is transferred, TETHNF and TEHNF are distinguished from one another by the average percent inaccuracy. When compared to the values of certain other factors, the percentage heat transmission rate for *Rd* is much higher at 15.8%. Regarding the topic of heat transfer, the actually calculated inaccuracy for the instance of *Q* comes in at 4.6%. These

factors all contribute to an increase in the heat transition factor that occurs when liquid travels through a stretched sheet that is well within a solar panel that is just on top of either a solar automobile or a solar panel. An improvement in the heat exchange phenomena that occurs within the photovoltaic solar vehicle and the solar array is brought about by an increase in the parameters that were discussed before.

Table 5 is designed in order to investigate the effects that a wide variety of factors have on C_f and *Nu* for TETHNF and TEHNF, a table like the one shown below has been drafted. The C_f increases when the porosity parameter λ, the Deborah number *De*, and the Casson parameter β are all given positive values. On the other hand, it decreases when the Reynolds number *Re* and the Sutterby viscosity parameter *M* have positive values. From the data shown in the table, it's indeed abundantly obvious that TETHNF provides superior outcomes when compared to TEHNF. Heat transport increases when *M*, heat production *Q*, thermal radiation *Rd*, and *Re* are present, while it decreases when a favorable variation in variant high thermal conductivity ε, Prandtl number *Pr*, *De*, λ, β is present. These factors enhance the efficiency of nanofluid across a stretched sheet that is situated within the photovoltaic panels of such electric vehicles. Throughout the event that the aforementioned requirements are satisfied, overall heat distribution within the thermal vehicle will see an improvement. The temperature, thermoelectric conductivity, and energy production of a hybrid liquid flow across a stretched sheet are all improved, and indeed, the photovoltaic solar-based vehicle can transport heat rather well.

4.1. Statistical interpretation of numerous assorted factors on skin friction and Nusselt number

Fig. 4(a–b) demonstrate a change in C_f that occurs when there is a significant fluctuation in a number of different factors. An object moving across a fluid might face opposition, known as frictional dragging," when it comes into direct contact with the surface of a liquid. This opposition may be experienced mostly by the object. Physically liquid behavior is termed compressing mostly in the event of an elevation in *De*, which offers a barrier to the movement of liquid over such material. A change in *De* causes a negative change in C_f. As seen in the image, it has been demonstrated beyond a reasonable doubt that the decrease in TETHNFs may predominate over the increases in TEHNF and HNF. The purpose of Fig. 4(b) is just to study the effect that TETHNFs, TEHNF in addition HNF have on C_f as a result of a change in *Re*. A hopeful development in *Re*'s character. Physically liquid thickness rises as a consequence of a rise in *Re*, which in turn causes the velocity distribution to decrease and C_f to improve in a manner that is inversely proportional to the effect of the velocity distribution.

Fig. 5(a–b) provide a pictorial depiction of the effect of the dimensionless numbers and *Rd* on the heat exchange rate. If a high-temperature gradient is required, thermal conductivity is one of the most important elements of *Rd.* Physically an increase in liquid temperature has been traced to the presence of radiation of a nonlinear nature, which has been shown to consist of *Rd*, but also *Pr*. As a result, as the temperature rises, so does the rate of heat transmission. In the case of TETHNF, the liquid temperature is higher than in the case of TEHNF and HNF. For instance, when Rd is amplified, the HT rate goes up. Electromagnetic waves may be thought of as the real medium via which radiation is transmitted. The heat of such a liquid is amplified as waves pass across it. Because of this, the rate of heat transmission increases as the magnifying *Rd* increases. Fig. 5(a–b) show that TETHNF is superior to TEHNF and HNF concerning heat transition.

4.2. Contour plots to investigate the influence of various sundry parameters on velocity and temperature profiles

Fig. 6(a) highlights the contour plot for velocity distribution against the porosity parameter λ. Enhancing the estimations of λ decelerates the velocity distribution. Physically porosity is linked with permeability. Fluid is not moving easily through the porous medium. Permeability of fluid flow increases enhancing λ amplifies liquid viscosity, in addition, depreciates fluid speed. Fig. 6(b) depicted the contour justifications of velocity against Deborah number *De*. It is observed that liquid viscosity decreases by improving *De*. The fluid changes its phase from liquid to solid by virtue of magnification in *De*. Physically fluid changes its behavior from liquid to solid due to an increment in viscosity under magnification in *De*. The viscosity factor in terms of liquid flow amplifies by improving *De* diminishing the velocity field as shown in Fig. 6(b). Fig. 7(a) presented the impact of *Rd* on the temperature profile in the form of a contour graph. The liquid temperature improves by augmenting *Rd*. More heat is absorbed by the fluid by magnifying Rd escalates temperature. Physically thermal radiation moves in the form of electromagnetic waves and carries heat with it which is absorbed by

Table 4
Skin friction coefficient against distinct parameters.

ε	*Pr*	*Q*	*Rd*	$Nu_x Re_x^{\frac{-1}{2}}$ Tetra nanoparticles	$Nu_x Re_x^{\frac{-1}{2}}$ Ternary nanoparticles	Relative error % $\frac{Nu_{tethnf} - Nu_{thnf}}{Nu_{tethnf}}$%
0.5	40	0.1	0.5	2.7125	2.4386	13.5 %
0.7				2.8875	2.5412	11.4 %
0.9				2.9018	2.6753	10.1 %
0.1				3.1579	2.8215	9.2 %
	41			2.8176	2.5321	13.2 %
	42			3.1213	2.9041	13.3 %
	43			3.5967	3.1651	13.5 %
		0.3		2.6178	2.3298	12.6 %
		0.5		2.8458	2.4176	12.4 %
		0.7		3.2475	2.7815	4.62 %
			1	3.2567	2.8765	14.3 %
			1.5	3.6487	3.1521	14.6 %
			2	4.1346	3.7331	15.8 %

Table 5
Skin friction and Nusselt number against distinct parameters.

λ	M	Re	ε	Pr	De	Q	Rd	β	$\frac{1}{2}Cf_xRe_x^{\frac{1}{2}}$ Ternary/EG	$\frac{1}{2}Cf_xRe_x^{\frac{1}{2}}$ Tetra/EG	$\frac{-1}{2}Nu_xRe_x^{\frac{1}{2}}$ Ternary/EG	$\frac{-1}{2}Nu_xRe_x^{\frac{1}{2}}$ Tetra/EG
0.5	0.5	0.1	0.5	40	0.1	0.1	0.5	0.5	1.8521	2.0123	3.4281	3.7251
1									1.9763	2.1516	3.6823	3.9013
1.5									2.1317	2.3679	3.8761	4.1206
	1								1.7563	1.8584	3.2171	3.5820
	1.5								1.7204	1.9801	3.3890	3.6129
	2								1.7013	1.9721	3.4156	3.6215
		0.3							1.7215	2.0156	3.4519	3.6712
		0.5							1.4821	1.6931	3.6820	3.8205
		0.6							1.2576	1.5056	3.8221	4.1089
			0.7						1.6870	1.8931	3.3543	3.6271
			0.9						1.6870	1.8931	3.3895	3.6542
			1.1						1.6870	1.8931	3.4762	3.7216
				41					1.6870	1.8931	3.6216	3.9219
				42					1.6870	1.8931	3.5401	3.8402
				43					1.6870	1.8931	2.8765	3.1784
					0.3				1.7086	1.8254	3.3785	3.5215
					0.5				1.8715	1.9115	3.1872	3.4182
					0.7				2.1216	2.3576	2.8019	3.0142
						0.3			1.6870	1.8931	3.3015	3.6215
						0.5			1.6870	1.8931	3.4219	3.7901
						0.7			1.6870	1.8931	3.6351	3.8631
							1		1.6870	1.8931	3.5081	3.7878
							1.5		1.6870	1.8931	3.7187	3.9213
							2		1.6870	1.8931	3.9213	4.1012
								1	1.8019	2.0213	3.6115	3.7095
								1.5	1.9136	2.1387	3.8076	4.0158
								2	2.1305	2.3140	4.1341	4.3987

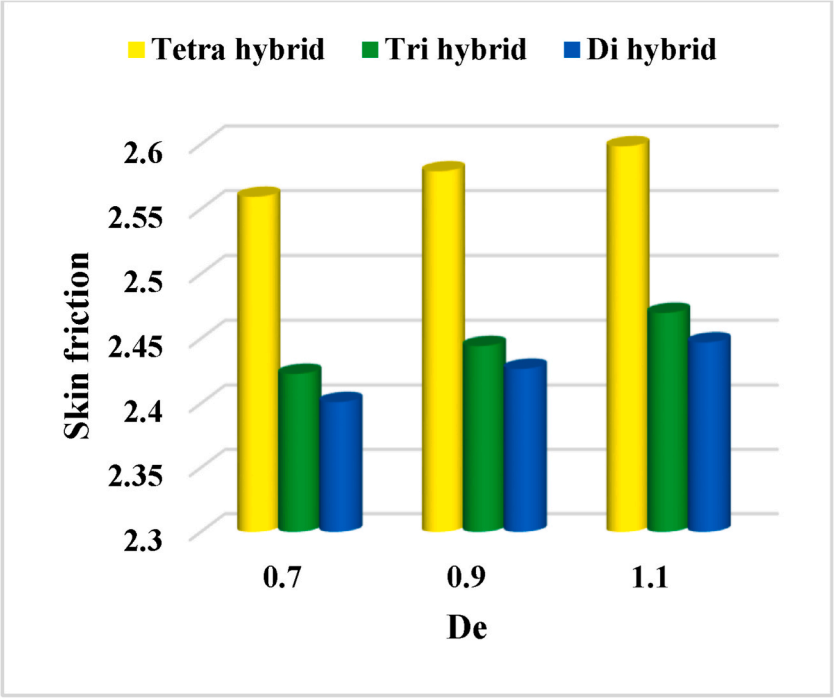

Fig. 4(a). Impact of *De* on the skin friction coefficient.

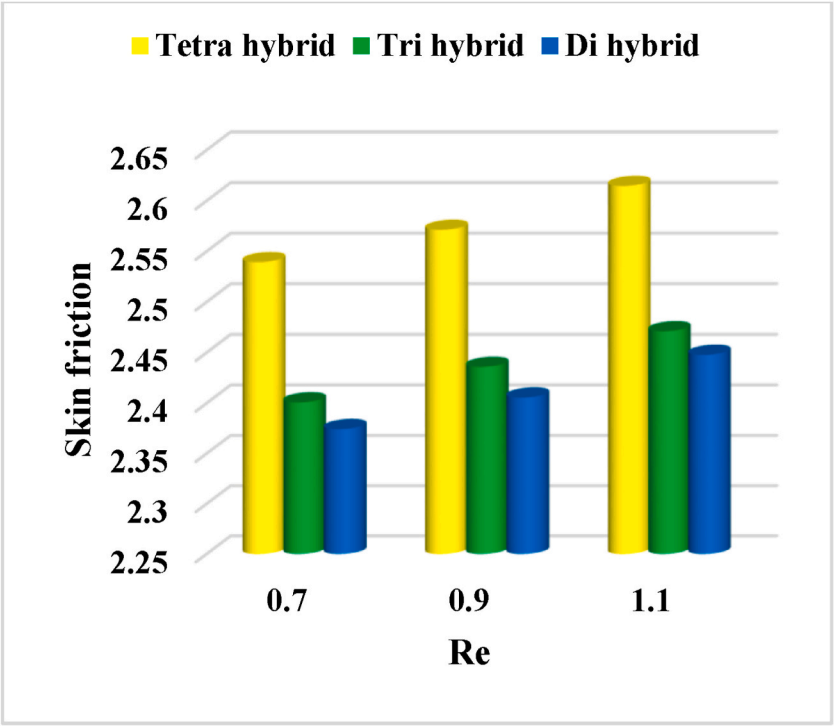

Fig. 4(b). Impact of *Re* on heat transfer Nusselt number.

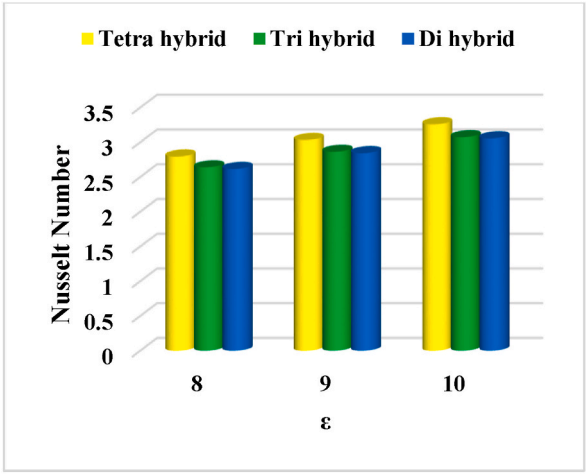

Fig. 5(a). Impact of ε on Nusselt number.

the fluid and amplifies the temperature of the fluid as well as the heat transport rate. The contour influence of the Prandtl number on the temperature profile is shown in Fig. 7(b). One can notice that the temperature distribution is de-increment with the incrementing estimations of the Prandtl number. The Prandtl number can be defined as momentum to thermal diffusivity. Physically heat diffuses more quickly by improving the Nusselt number which diminishes $\theta(\eta)$.

5. Quadratic regression analysis in the case of Nusselt number

Throughout the process of regression analysis, the other distinguishing parameters are locked in place. This happens throughout the process of regression analysis. In the context of heat transfer, the numerical quantities associated with Nu_x have been partitioned into 110 distinct groups according to their respective values of ε in addition to *Rd*. The other parameters all have values that fall within the ranges of [0.05 and 0.5] and [0.05 and 0.20], respectively. The following are the representations of the mathematical expressions

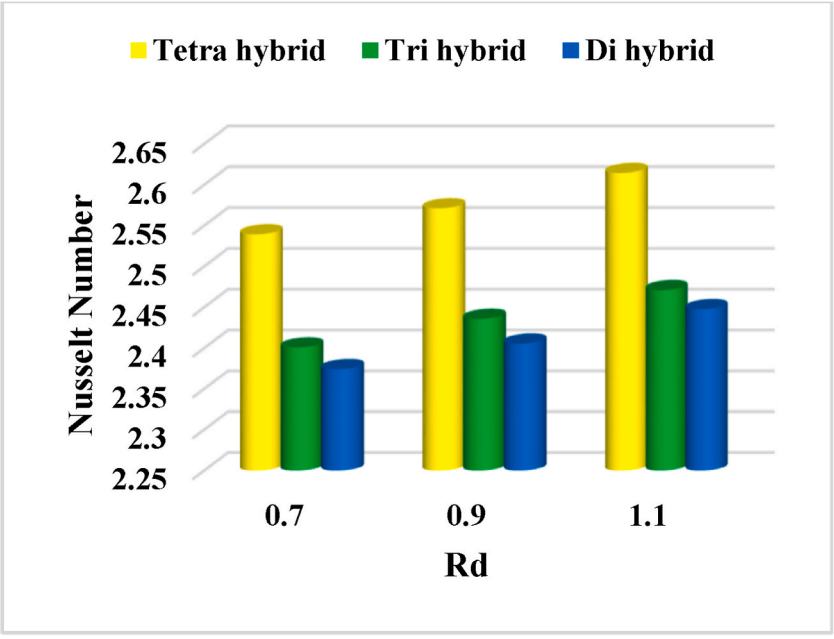

Fig. 5(b). Impact of *Rd* on heat transfer Nusselt number.

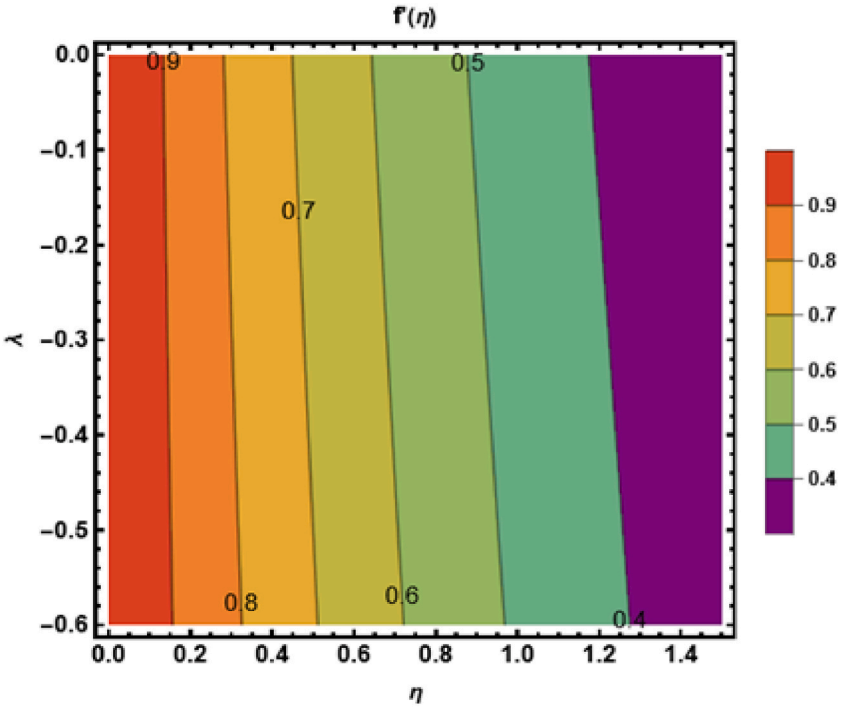

Fig. 6(a). Stream lines plot of Porosity parameter λ against velocity field.

of the quadratic regression model:

$$Nu_{qre} = Nu_x + c_1\varepsilon + c_2 Rd + c_3\varepsilon^2 + c_4 Rd^2 + c_5\varepsilon Rd. \tag{26}$$

On the other hand, c_1, c_2, c_3, c_4, c_5 are approximations of the values of Nu_x that were numerically determined using the regression analysis approach indicated in Table 6. The equation $\varepsilon_n = \frac{|Nu_{qre} - Nu_x|}{Nu_x}$ is used to do the computations necessary to carry out the analysis of

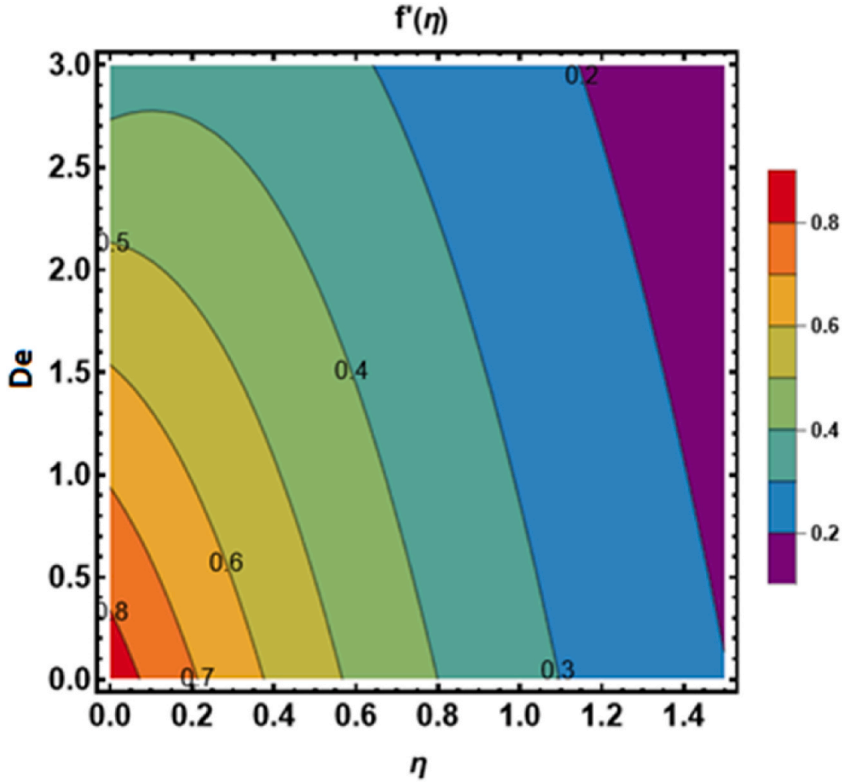

Fig. 6(b). Stream lines plot of Deborah number *De* against velocity field.

errors for the value of Nu_x. It can be seen from Table 6 that there is a reduction in the amount of error that occurs when heat is transferred due to amplification in ε as well as *Rd*.

6. Concluding remarks

This article presents a new way of thinking about the entropy production and heat transport analyses of photovoltaic hybrid vehicles, by factoring Casson-Sutterby liquid. Comprehensive research on the effects of various factors on the hybrid solar automobile is presented throughout in terms of charts and graphs. The following is a brief overview of the most important parts of the aforementioned study.

1) For the case of different factors, *Rd*, *Q*, *M* on TETHNF, heat distribution phenomena within solar automobiles improve.
2) Past an expandable sheet in solar automobiles, TETHNF is a more efficient heat source than TEHNF and HNF.
3) A magnification in porosity λ and Deborah *De* diminishes the velocity distribution.
4) When *Q*, *Rd*, and ε are magnified, the heat transport phenomenon amplifies
5) The temperature distribution phenomena within the solar automobile are bolstered by thermal radiations *Rd* falling on the surface of an expandable sheet located inside a photovoltaic solar panel.
6) Relative percentage error diminishes from 12.6% to 4.62% in the case of heat transfer Nusselt number by the virtue of magnification in heat generation parameter from $0.3 \leq Q \leq 0.7$.
7) Relative percentage error amplifies from 14.3% to 15.8% in the case of heat transport Nusselt as a result of amplification in thermal radiation phenomenon from $1 \leq Rd \leq 2$.
8) Regression error analysis diminishes from 0.0185 to 0.0151 in the case of magnification in *Rd* from 2 to 2.5 by keeping $\varepsilon = 1.5$ fixed.
9) Relative percentage error is minimum amplifies from 14.3% to 15.8% in the case of heat transport Nusselt as a result of amplification in thermal radiation phenomenon from $1 \leq Rd \leq 2$.
10) Agglomeration of nanoparticles in the base fluid amplifies the heat transfer rate from 3.2567 to 4.1346 in contrast to ternary nanoparticles 2.8765 to 3.7331 owing to magnification in *Rd* from 1 to 2.

Author contributions

TS, WJ and MRE formulated the problem. WJ and MRE solved the problem. TS, WJ, NMK, MRE, AAE, NSEA, SMED and GCA computed and scrutinized the results. All the authors equally contributed in writing and proof reading of the paper. All authors

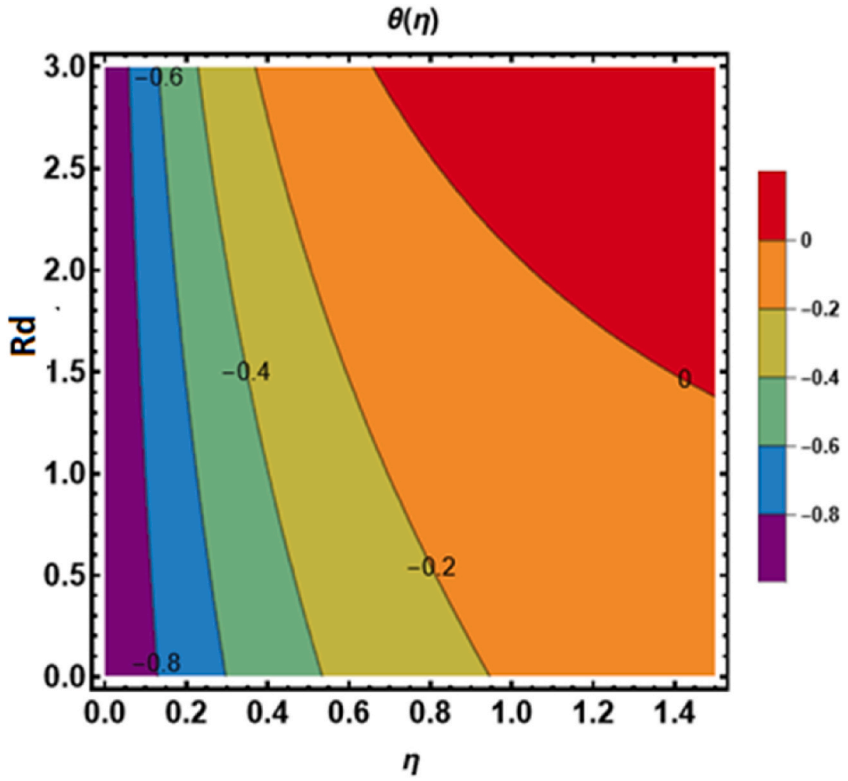

Fig. 7(a). Stream lines plot of thermal radiation *Rd* against temperature field.

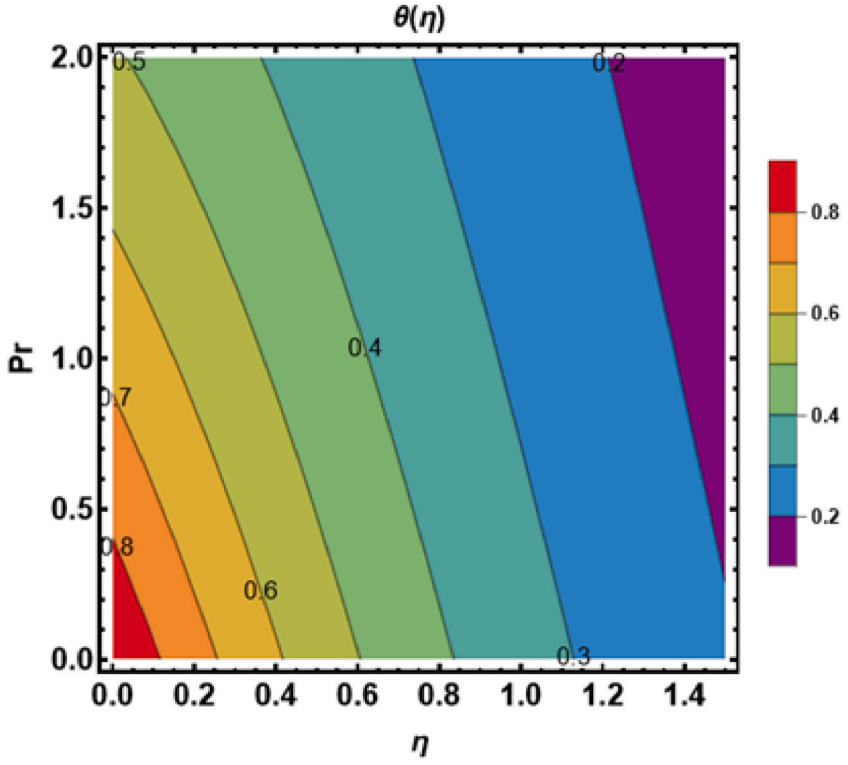

Fig. 7(b). Stream lines plot of Prandtl number *Pr* against temperature field.

Table 6
Error analysis for the case of Nu_x by improving ε and Rd.

ε	Rd	Nu_x	c_1	c_2	c_3	c_4	c_5	ε_1
1.5	2	3.1576	0.0412	−0.0331	−0.0315	0.0311	0.1601	0.0185
1.5	2.5	3.2173	0.0051	−0.0612	−0.0005	0.0501	0.1723	0.0151
2.5	2	3.5219	0.0200	−0.0765	0.0007	0.2341	0.1583	0.0450
2.5	2.5	3.5331	0.0061	−0.0815	0.0270	0.2389	0.1506	0.0400

reviewed the manuscript.

Declaration of competing interest

The authors declare that they have no known competing financial interests or personal relationships that could have appeared to influence the work reported in this paper.

Data availability

Data will be made available on request.

Acknowledgements

The authors extend their appreciation to the Deanship of Scientific Research at King Khalid University for funding this work through large group Research Project under grant number **RGP2/441/44**.

Nomenclature

Re	Reynold's number
T_0	wall temperature
Ω	temperature gradient
B	electromagnetic parameter
Ec	Eckert number
Nu_x	Nusselt number
Pr	Prandtl number
Q	heat generation parameter
τ	shear stress
ρ_{hnf}	hybrid nanofluid density
C_p	specific heat at constant pressure
σ^*	Stefan-Boltzmann constant
De	Deborah number
T_∞	ambient temperature
λ	porosity parameter
ε	variant thermal conductance
Cf_x	Skin friction
Rd	radiation parameter
q_r	radiative heat flux
τ_s	reference shear stress
α_{hnf}	hybrid nanofluid thermal diffusivity
k_{hnf}	hybrid thermal conductivity
κ^*	absorption coefficient

References

[1] X. Wang, Y. He, X. Liu, L. Shi, J. Zhu, Investigation of photothermal heating enabled by plasmonic nanofluids for direct solar steam generation, Sol. Energy 157 (2017) 35–46.
[2] X. Wang, Y. He, X. Liu, J. Zhu, Enhanced direct steam generation via a bio-inspired solar heating method using carbon nanotube films, Powder Tech 321 (2017) 276–285.
[3] X. Wang, Y. He, X. Liu, J. Zhu, Solar steam generation through bioinspired interface heating of broadband-absorbing plasmonic membranes, Appl. Energy 195 (2017) 414–425.
[4] X. Wang, Y. He, X. Liu, J. Zhu, Direct vapor generation through localized solar heating via carbon-nanotube nanofluid, Energy Conv. Manag. 130 (2016) 176–183.

[5] N. Mazaheri, S. Khanmohammadi, M. Bahiraei, Z. Said, Two-phase simulation of the generated entropy for the nanofluid flow inside a ribbed passage for cooling of a PV cell, Thermal Sci. Eng. Prog. 33 (2022), 101353.
[6] A.K. Hamzat, M.I. Omisanya, A.Z. Sahin, O.R. Oyetunji, N.A. Olaitan, Application of nanofluid in solar energy harvesting devices: a comprehensive review, Energy Conv. Manag. 266 (2022), 115790.
[7] S.U.S. Choi, Enhancing thermal conductivity of fluids with nanoparticles, Developments and Application of Non-Newtonian Flows 66 (1995) 99–105.
[8] H. Masuda, A. Ebata, K. Teramae, Alteration of thermal conductivity and viscosity of liquid by dispersing ultra-fine particles by dispersion of Al_2O_3, SiO_2 and TiO_2 ultra-fine particles, Netsu Bussei 7 (1993) 227–233.
[9] J.A. Eastman, S. Choi, S. Li, W. Yu, L. Thompson, Anomalously increased effective thermal conductivities of ethylene glycol-based nanofluids containing copper nanoparticles, Appl. Phys. Lett. 78 (6) (2001) 718–720.
[10] M.R. Eid, A. Al-Hossainy, M.S. Zoromba, FEM for blood-based SWCNTs flow through a circular cylinder in a porous medium with electromagnetic radiation, Commun. Theoret. Phys. 71 (12) (2019) 1425.
[11] S. Lahmar, M. Kezzar, M.R. Eid, M.R. Sari, Heat transfer of squeezing unsteady nanofluid flow under the effects of an inclined magnetic field and variable thermal conductivity, Physica A 540 (2020), 123138.
[12] M.R. Eid, M.A. Nafe, Thermal Conductivity Variation and Heat Generation Effects on Magneto-Hybrid Nanofluid Flow in a Porous Medium with Slip Condition, Waves Random Complex Media, 2020, pp. 1–25, https://doi.org/10.1080/17455030.2020.1810365.
[13] S.A. Adio, M. Sharifpur, J.P. Meyer, Factors affecting the pH and electrical conductivity of MgO–ethylene glycol nanofluids, Bull. Mater. Sci. 38 (5) (2015) 1345–1357.
[14] S.N. Shoghl, J. Jamali, M.K. Moraveji, Electrical conductivity, viscosity, and density of different nanofluids: an experimental study, Experim. Therm. Fluid Sci. 74 (2016) 339–346.
[15] S.F.M. Nor, N. Azis, J. Jasni, M.Z.A. Ab Kadir, R. Yunus, Z. Yaakub, Investigation on the electrical properties of palm oil and coconut oil based TiO_2 nanofluids, IEEE Trans. Dielec. Elect. Insul. 24 (6) (2017) 3432–3442.
[16] M. Milanese, G. Colangelo, A. Cretì, M. Lomascolo, F. Iacobazzi, A. de Risi, Optical absorption measurements of oxide nanoparticles for application as nanofluid in direct absorption solar power systems – Part I: water-based nanofluids behavior, Sol. Energy Mater. Sol. Cell. 147 (2016) 315–320.
[17] M. Milanese, G. Colangelo, A. Cretì, M. Lomascolo, F. Iacobazzi, A. de Risi, Optical absorption measurements of oxide nanoparticles for application as nanofluid in direct absorption solar power systems – Part II: ZnO, CeO_2, Fe_2O_3 nanoparticles behavior, Sol. Energy Mater. Sol. Cell. 147 (2016) 321–326.
[18] M. Milanese, F. Iacobazzi, G. Colangelo, A. de Risi, An investigation of layering phenomenon at the liquid–solid interface in Cu and CuO based nanofluids, Int. J. Heat Mass Tran. 103 (2016) 564–571.
[19] F. Iacobazzi, M. Milanese, G. Colangelo, M. Lomascolo, A. de Risi, An explanation of the Al_2O_3 nanofluid thermal conductivity based on the phonon theory of liquid, Energy 116 (2016) 786–794.
[20] G. Colangelo, M. Milanese, Numerical simulation of thermal efficiency of an innovative Al_2O_3 nanofluid solar thermal collector influence of nanoparticles concentration, Therm. Sci. 21 (2017) 2769–2779.
[21] M. Potenza, M. Milanese, G. Colangelo, Arturo de Risi, Experimental investigation of transparent parabolic trough collector based on gas-phase nanofluid, Applied, Energy 203 (2017) 560–570.
[22] G. Colangelo, E. Favale, M. Milanese, A. de Risi, D. Laforgia, Cooling of electronic devices: nanofluids contribution, Appl. Therm. Eng. 127 (2017) 421–435.
[23] G. Colangelo, E. Favale, P. Miglietta, M. Milanese, A. de Risi, Thermal conductivity, viscosity and stability of Al_2O_3-diathermic oil nanofluids for solar energy systems, Energy 95 (2016) 124–136.
[24] G. Colangelo, E. Favale, M. Milanese, G. Starace, A. De Risi, Experimental measurements of Al_2O_3 and CuO nanofluids interaction with microwaves, J. Energy Eng. 143 (2) (2017), 04016045.
[25] F. Iacobazzi, M. Milanese, G. Colangelo, A. de Risi, A critical analysis of clustering phenomenon in Al_2O_3 nanofluids, Journal of Thermal Analysis and Calorimetry 135 (2019) 371–377.
[26] G. Colangelo, N.F. Diamante, M. Milanese, G. Starace, A. de Risi, A critical review of experimental investigations about convective heat transfer characteristics of nanofluids under turbulent and laminar regimes with a focus on the experimental setup, Energies 14 (2021) 6004.
[27] Adun Humphrey, Doga Kavaz, Mustafa Dagbasi, Review of ternary hybrid nanofluid: synthesis, stability, thermophysical properties, heat transfer applications, and environmental effects, J. Clean. Prod. 328 (2021), 129525.
[28] K.N. Sneha, G.P. Vanitha, U.S. Mahabaleshwar, D. Laroze, Effect of couple stress and mass transpiration on ternary hybrid nanoliquid over a stretching/shrinking sheet with heat transfer, Micromachines 13 (2022) 1694.
[29] J. Suresh Goud, Pudhari Srilatha, R.S. Varun Kumar, K. Thanesh Kumar, Umair Khan, Zehba Raizah, Harjot Singh Gill, Ahmed M. Galal, Role of ternary hybrid nanofluid in the thermal distribution of a dovetail fin with the internal generation of heat, Case Stud. Therm. Eng. 35 (2022), 102113.
[30] S. Nasir, S. Sirisubtawee, P. Juntharee, et al., Heat transport study of ternary hybrid nanofluid flow under magnetic dipole together with nonlinear thermal radiation, Appl. Nanosci. 12 (2022) 2777–2788.
[31] W. Cao, I.L. Animasaun, Se-Jin Yook, V.A. Oladipupo, Xianjun Ji, Simulation of the dynamics of colloidal mixture of water with various nanoparticles at different levels of partial slip: ternary-hybrid nanofluid, Int. Commun. Heat Mass Transf. 135 (2022), 106069.
[32] Z. Mahmood, Z. Iqbal, M.A. Alyami, B. Alqahtani, M.F. Yassen, U. Khan, Influence of suction and heat source on MHD stagnation point flow of ternary hybrid nanofluid over convectively heated stretching/shrinking cylinder, Adv. Mech. Eng. 14 (9) (2022) 1–17.
[33] A. Mojiri, R. Taylor, E. Thomsen, G. Rosengarten, Spectral beam splitting for efficient conversion of solar energy-a review, Renew. Sustain. Energy Rev. 28 (2013) 654–663.
[34] Z. Said, A. Mehmood, Standalone photovoltaic system assessment for major cities of United Arab Emirates based on simulated results, J. Clean. Prod. 140 (2017) 2722–2729.
[35] Z. Said, A.A. Alshehhi, A. Mehmood, Predictions of UAE's renewable energy mix in 2030, Renew. Energy 118 (2018) 779–789.
[36] E. Bellos, Progress in the design and the applications of linear fresnel re-flectorsea critical review, Thermal Sci. Eng. Prog. 10 (2019) 112–137.
[37] M. Ghodbane, E. Bellos, Z. Said, B. Boumeddane, A. Khechekhouche, M. Sheikholeslami, Z.M. Ali, Energy, financial, and environmental investigation of a direct steam production power plant driven by linear fresnel solar reflectors, J. Sol. Energy 143 (2020), 021008.
[38] M. Ghodbane, B. Boumeddane, Z. Said, E. Bellos, A numerical simulation of a linear Fresnel solar reflector directed to produce steam for the power plant, J. Clean. Prod. 231 (2019) 494–508.
[39] G.A. Gonzalez, M.C. Pereira, F. Cuadros, T. Fartaria, Energy self-sufficiency through hybridization of biogas and photovoltaic solar energy: an application for an Iberian pig slaughterhouse, J. Clean. Prod. 65 (2014) 318–323.
[40] E. Kabir, P. Kumar, S. Kumar, A.A. Adelodun, K. Kim, Solar energy: potential and future prospects, Renew. Sustain. Energy Rev. 82 (2014) 894–900.
[41] N. Kannan, D. Vakeesan, Solar energy for future world: a review, Renew. Sustain. Energy Rev. 52 (2016) 1092–1105.
[42] C. Luan, Z. Liu, X. Wang, Divergence and convergence: technology- relatedness evolution in solar energy industry, Scientometrics 97 (2013) 461–475.
[43] Y.A. Qandile, M.I. Sabry, Guidelines for the treatment of solar energy topics in the unified science curricula of the Gulf Arab states, Renew. Energy 14 (1998) 401–414.
[44] R. Quitzow, J. Huenteler, H. Asmussen, Development trajectories in China's wind and solar energy industries: how technology-related differences shape the dynamics of industry localization and catching up, J. Clean. Prod. 158 (2017) 122–133.
[45] J. Zhang, Y. Yan, J. Guan, Scientific relatedness in solar energy: a comparative study between the USA and China, Scientometrics 102 (2015) 1595–1613.
[46] E.A. Algehyne, H.F. Alrihieli, M. Bilal, A. Saeed, W. Weera, Numerical approach toward ternary hybrid nanofluid flow using variable diffusion and non-fourier's concept, ACS Omega 7 (33) (2022) 29380–29390.
[47] T. Sajid, A. Ayub, S.Z.H. Shah, W. Jamshed, M.R. Eid, E.M. El Din, R. Irfan, S.M. Hussain, Trace of chemical reactions accompanied with arrhenius energy on ternary hybridity nanofluid past a wedge, Symmetry 14 (2022) 1850.

[48] F. Wang, U. Nazir, M. Sohail, E.R. El-Zahar, C. Park, P. Thounthong, A Galerkin strategy for tri-hybridized mixture in ethylene glycol comprising variable diffusion and thermal conductivity using non-Fourier's theory, Nanotechnol. Rev. 11 (1) (2022) 834–845.
[49] T. Sajid, W. Jamshed, R.W. Ibrahim, M.R. Eid, A. Abd-Elmonem, M. Arshad, Quadratic regression analysis for nonlinear heat source/sink and mathematical Fourier heat law influences on Reiner-Philippoff hybrid nanofluid flow applying Galerkin finite element method, Journal of Magn. Magn. Mater. 568 (2023), 170383.
[50] C. Zhao, S. Zheng, J. Zhang, Y. Zhang, Exergy and economic analysis of organic Rankine cycle hybrid system utilizing biogas and solar energy in rural area of China, Int. J. Green Energy 14 (2017), 123437.
[51] W. Jamshed, Numerical investigation of MHD impact on Maxwell nanofluid, Int. Commun. Heat Mass Tran. 120 (2021), 104973.
[52] I. Waini, N.S. Khashi'ie, A.R.M. Kasim, N.A. Zainal, A. Ishak, I. Pop, Radiative heat transfer of Reiner–Philippoff fluid flow past a nonlinearly shrinking sheet: Dual solutions and stability analysis, Chin. J. Phys. 77 (2022) 45–56.